



Article

SKAP interacts with Aurora B to guide end-on capture of spindle microtubules via phase separation

Manjuan Zhang^{1,2,†}, Fengrui Yang^{1,2,3,†}, Wenwen Wang^{1,3}, Najdat Zohbi³, Xiwei Wang^{1,2,3}, Dongmei Wang^{1,2,3}, Xiaoxuan Zhuang¹, Zhen Dou ^{1,2}, Dan Liu¹, Xiaoyu Song^{1,2,3}, Hadiyah-Nicole Green³, Xing Liu ^{1,*}, and Xuebiao Yao^{1,*}

¹ MOE Key Laboratory for Cellular Dynamics and Hefei National Laboratory for Physical Sciences at the Microscale, University of Science and Technology of China, Hefei 230027, China

² Anhui Key Laboratory for Cellular Dynamics and Chemical Biology and CAS Center for Excellence in Molecular Cell Science, Hefei 230027, China

³ Keck Center for Organoids Plasticity Control, Morehouse School of Medicine, Atlanta, GA 30310, USA

[†] These authors contributed equally to this work.

* Correspondence to: Xing Liu, E-mail: xing1017@ustc.edu.cn; Xuebiao Yao, E-mail: yaorb@ustc.edu.cn

Edited by Haian Fu

Chromosome segregation in mitosis is orchestrated by the dynamic interactions between the kinetochore and spindle microtubules. Our recent studies show that mitotic motor CENP-E cooperates with SKAP and forms a link between kinetochore core MIS13 complex and spindle microtubule plus-ends to achieve accurate chromosome alignment in mitosis. However, it remains elusive how SKAP regulates kinetochore attachment from lateral association to end-on attachment during metaphase alignment. Here, we identify a novel interaction between Aurora B and SKAP that orchestrates accurate interaction between the kinetochore and dynamic spindle microtubules. Interestingly, SKAP spontaneously phase-separates *in vitro* via weak, multivalent interactions into droplets with fast internal dynamics. SKAP and Aurora B form heterogeneous coacervates *in vitro*, which recapitulate the dynamics and behavior of SKAP comets *in vivo*. Importantly, SKAP interaction with Aurora B via phase separation is essential for accurate chromosome segregation and alignment. Based on those findings, we reason that SKAP–Aurora B interaction via phase separation constitutes a dynamic pool of Aurora B activity during the lateral to end-on conversion of kinetochore–microtubule attachments to achieve faithful cell division.

Keywords: Aurora B, SKAP, kinase activity, mitosis, phase separation

Introduction

Error-free mitosis depends on accurate chromosome attachment to spindle microtubules, end-on capture of kinetochore microtubules, and powered congression of those chromosomes prior to chromatid segregation in anaphase (Cleveland et al., 2003; Foley and Kapoor, 2013; McKinley and Cheeseman, 2016; Liu et al., 2020). Accurate chromosome attachment to lateral spindle microtubules and subsequent conversion to end-on capture are essential for genomic stability in mitosis (Shrestha et al., 2017; Huang et al., 2019). The kinetochore

acts as a structural platform for linking the centromere to spindle microtubules and functions as a signaling hub coordinating chromosome attachment and the metaphase-to-anaphase transition (Bakhom et al., 2009a, b; Cheeseman, 2014; McKinley and Cheeseman, 2016). Mounting evidence supports the critical role of KNL1–Mis12–Ndc80 complex in coupling spindle microtubule plus-ends to the kinetochore (Cheeseman and Desai, 2008; DeLuca, 2010; Foley and Kapoor, 2013; Hara and Fukagawa, 2017). However, using recombinant human kinetochore components, it was shown that single NDC80 complexes do not track depolymerizing microtubules (Volkov et al., 2018). An efficient coupling requires three or more NDC80 complexes bound to CENP-T, suggesting the importance of multivalency in end-on capture of kinetochore microtubules.

An early search for conversion of lateral to end-on capture regulators has led to the identification of SKAP as an outer

Received April 10, 2021. Revised June 15, 2021. Accepted June 21, 2021.

© The Author(s) (2021). Published by Oxford University Press on behalf of *Journal of Molecular Cell Biology*, CEMCS, CAS.

This is an Open Access article distributed under the terms of the Creative Commons Attribution-NonCommercial License (<https://creativecommons.org/licenses/by-nc/4.0/>), which permits non-commercial re-use, distribution, and reproduction in any medium, provided the original work is properly cited. For commercial re-use, please contact journals.permissions@oup.com

kinetochore protein that is essential for chromosome alignment (Fang et al., 2009; Wang et al., 2012). SKAP forms functional complexes with Astrin and the mitotic kinesin CENP-E, respectively (Thein et al., 2007; Huang et al., 2012). Our early study showed that SKAP cooperates with CENP-E to orchestrate kinetochore–microtubule interaction for faithful chromosome segregation (Huang et al., 2012). Interestingly, suppression of CENP-E does not abolish the kinetochore localization of SKAP, raising interest in the identification of the kinetochore constituent(s) that specifies SKAP localization to the kinetochore. Indeed, our follow-up study showed that SKAP interacts with MIS13 and this interaction specifies the kinetochore localization of SKAP (Wang et al., 2012), which functions as a linker protein connecting the outer kinetochore with dynamic microtubule plus-ends.

Liquid–liquid phase separation (LLPS) is an emerging property for organizing multivalent membraneless organelle to achieve high local concentration for prompt catalysis with precise spatio-temporal control (Li et al., 2012; Hyman et al., 2014; Banani et al., 2017). Recent study showed that LLPS-driven compartmentalization at the inner centromeres involves Aurora B kinase, INCENP, survivin, and borealin (Woodruff et al., 2017; Woodruff, 2018; So et al., 2019; Trivedi et al., 2019). Aurora B is the key component of chromosome passenger complex, playing a critical role in destabilizing aberrant microtubule–kinetochore connection through phosphorylating numbers of kinetochore factors (Trivedi et al., 2019). Our recent studies identified a signaling axis in which Aurora B activity is modulated by CDK1 via the acetyltransferase TIP60 in human cell division (Mo et al., 2016; Zachos, 2016; Bao et al., 2018; Yang and Yu, 2018). Interestingly, TIP60 cooperates with Aurora B at the outer kinetochore to regulate the dynamic interactions between Ndc80 and spindle microtubules via post-translational modifications of Hec1 (Zhao et al., 2019), which suggests that Aurora B functions at different subcompartments at the centromere and the kinetochore. We therefore speculated that phase separation underlies compartmentalization at outer kinetochores. Next, we sought to search for proteins that initiate LLPS for Aurora B compartmentalization at the outer kinetochore and are required for transition from lateral attachment to end-on capture during mitosis.

Here, we demonstrate that SKAP can undergo phase separation *in vitro* and exists in a phase-separated state at the kinetochore. We also demonstrate that the ability of SKAP to undergo phase separation is important for its interaction and specification of Aurora B at the kinetochore. We reason that the LLPS-driven SKAP interaction with Aurora B guides end-on capture of spindle microtubules, which is essential for metaphase alignment in mitosis.

Results

SKAP is essential for optimal Aurora B activity in mitosis

Our early studies showed that MIS13 interacts with SKAP and Aurora B during mitosis (Yang et al., 2008; Wang et al., 2012).

However, there is no direct link between SKAP and Aurora B in mitosis. To explore the link between SKAP and Aurora B, a co-immunoprecipitation (co-IP) assay was carried out and confirmed that SKAP formed a complex with Aurora B *in vivo* (Figure 1A). Consistently, the direct interaction between SKAP and Aurora B *in vitro* was confirmed by a pull-down assay in which His-green fluorescent protein (GFP)-SKAP interacted with GST-Aurora B rather than GST (Supplementary Figure S1A).

To further explore the functional relationship between SKAP and Aurora B, we examined the phenotype in cells deficient in SKAP using siRNA-mediated knockdown approach (Wang et al., 2012). As shown in Figure 1B and Supplementary Figure S1B, suppression of SKAP resulted in reduction of Aurora B activity, judged by localization of pSer10-histone 3 (pS10-H3) and pThr232-Aurora B (pT232-Aurora B), similar to what was seen in Aurora B-inhibited (ZM447439) cells. Quantitative analyses of Aurora B activity at the kinetochore judged by pS10-H3 and pT232-Aurora B levels indicated that SKAP is essential for Aurora B activity at the kinetochore (Figure 1C; Supplementary Figure S1C). Consistently, western blotting analyses also show that suppression of SKAP resulted in reduction of Aurora B activity, judged by the levels of pS10-H3 and pT232-Aurora B (Figure 1D).

To elucidate the precise function of SKAP in chromosome segregation in mitosis, we examined the resulting mitotic phenotype using time-lapse microscopy. Although cells treated with control siRNA progressed normally through mitosis, SKAP-depleted cells showed a high frequency of chromosome segregation defects, including chromosome misalignment, anaphase lagging chromosomes, and chromosome bridges (Figure 1E), demonstrating the role of SKAP in mitotic chromosome movements. Statistical analyses show that SKAP is essential for accurate chromosome segregation, as suppression of SKAP resulted in chromosome misalignment, anaphase lagging chromosomes, and chromosome bridges (Figure 1F–H). The chromosome segregation errors seen in SKAP-deficient cells phenocopied the mitotic abnormalities seen in Aurora B-inhibited cells, suggesting potential interactions between SKAP and Aurora B.

SKAP undergoes phase separation in vitro

To examine whether SKAP interacts with Aurora B, we sought to purify bacterially recombinant SKAP. Surprisingly, full-length recombinant SKAP protein often precipitates during desalting step. Thus, we sought to characterize whether SKAP possesses LLPS property using GFP-SKAP purified from *Escherichia coli* (Figure 2A and B). We observed spontaneous SKAP phase separation at 10 μ M under very low salt concentration (BRB80 buffer) in the absence of the molecular crowding agent (PEG-8000) (Figure 2C). The presence of molecular crowding agent (PEG-8000) significantly promoted SKAP phase separation under conditions of low protein concentration (2.5 μ M) (Figure 2C; Supplementary Figure S2A). Coacervates formed from GFP-tagged SKAP were fluorescent, demonstrating that they are composed of SKAP protein (Figure 2C). Real-time

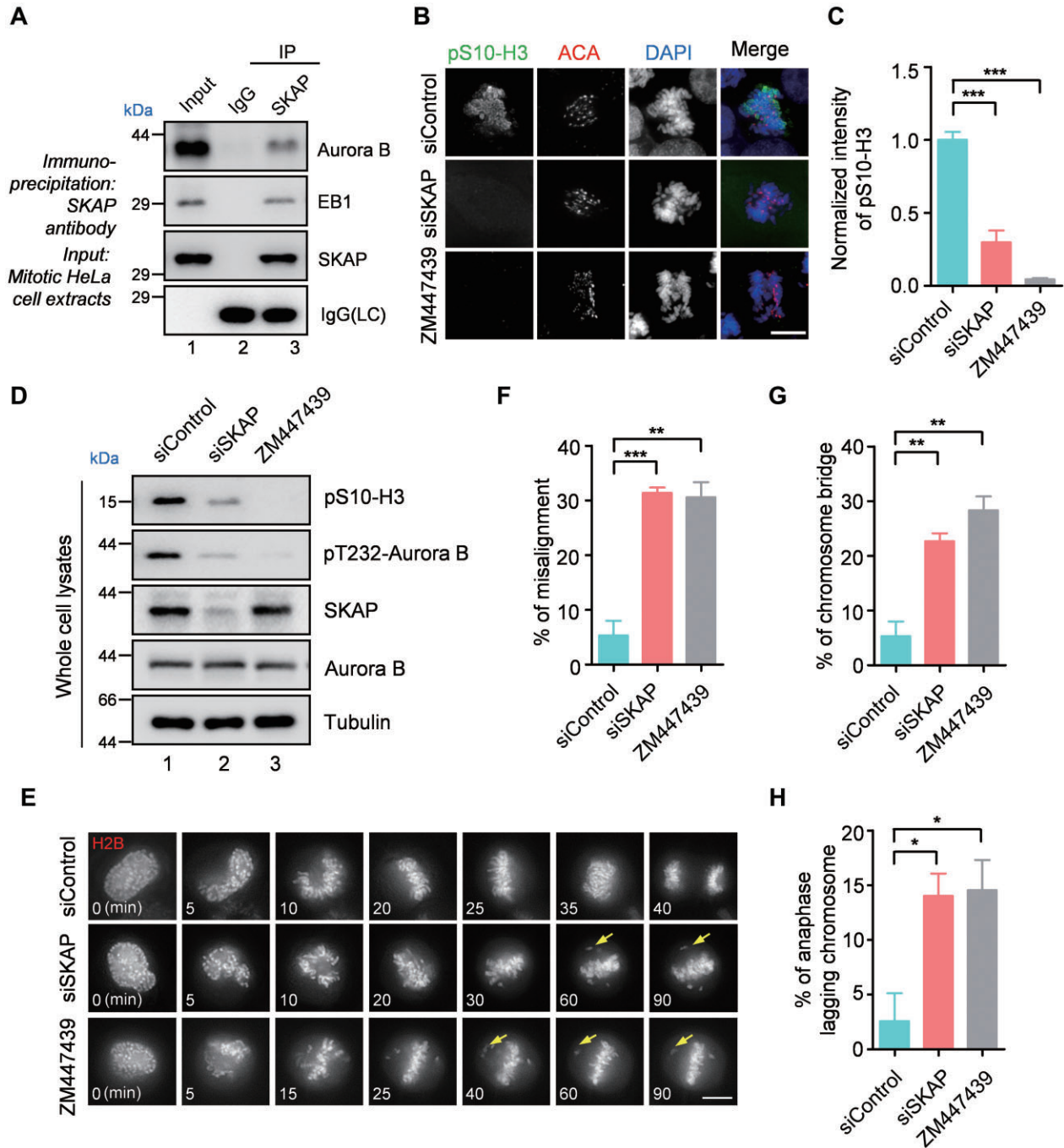


Figure 1 SKAP is essential for Aurora B kinase activation. **(A)** Mitotic HeLa cells were subjected to IP with SKAP antibody or IgG. Immunoprecipitates were blotted with Aurora B, SKAP, and EB1 antibodies. Note that SKAP brought down EB1 and Aurora B. **(B)** Representative immunofluorescence images of HeLa cells stained with pS10-H3 (green) and ACA (red). DNA was stained with DAPI (blue) to observe chromosomes. Cells were transfected with SKAP or control siRNA for 48 h or treated with ZM447439 for 45 min before fixation. Scale bar, 10 μ m. **(C)** Statistical analysis of fluorescence intensity in **B**. Data represent mean \pm SEM from three independent experiments. **(D)** HeLa cells were transfected with control or SKAP siRNA for 48 h or treated with ZM447439 for 45 min before harvest. Whole cell lysates were separated by SDS-PAGE and blotted with pS10-H3, pT232-Aurora B, SKAP, Aurora B, and tubulin antibodies. Tubulin was used as a loading control. **(E)** Real-time imaging of mitotic phenotypes of HeLa cells transfected with control or SKAP siRNA or treated with ZM447439 were shown by DeltaVision time-lapse microscopy, visualized with mCherry-H2B (H2B in red color) (arrows, misalignment; numbers at bottom left of images indicate elapsed time in minutes). Scale bar, 10 μ m. **(F–H)** Quantification of chromosome segregation defects of live HeLa cells expressing siControl ($n = 35$) or siSKAP ($n = 35$) or treated with ZM447439 ($n = 34$). Data are mean \pm SEM. Statistical significance was tested by two-sided *t*-test; * $P < 0.05$, ** $P < 0.01$, *** $P < 0.001$.

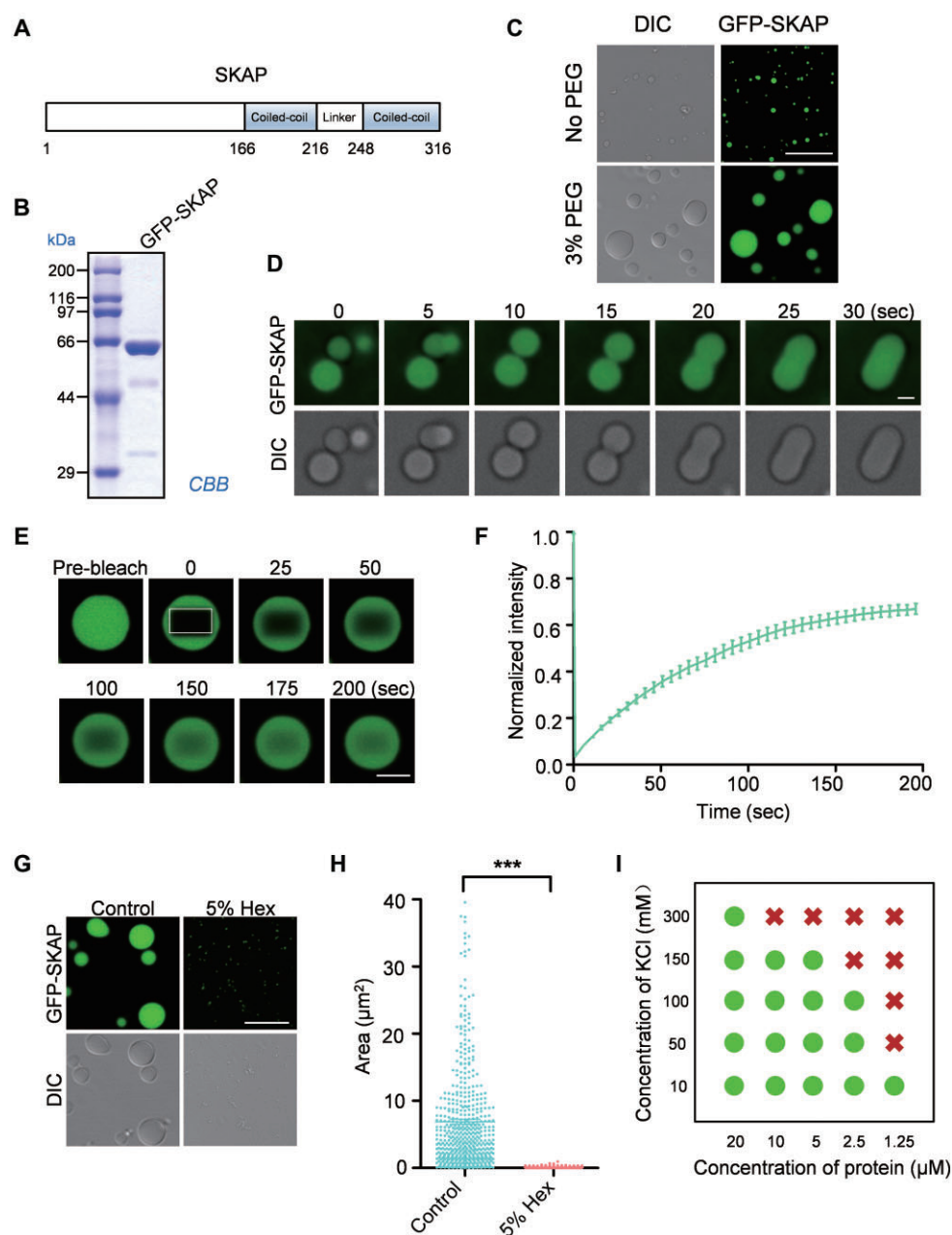


Figure 2 SKAP undergoes phase separation *in vitro*. **(A)** Schematic diagram of domain structure of SKAP. Residue numbers at domain boundaries are indicated. **(B)** Coomassie Brilliant Blue-stained SDS-PAGE gel of purified recombinant His-GFP-SKAP proteins from *E. coli*. **(C)** Phase separation of GFP-SKAP ($10\ \mu\text{M}$ in BRB80 buffer) occurs with or without PEG (3% PEG-8000), leading to liquid droplets observable by DIC and fluorescent ($\lambda 488\ \text{nm}$) microscopy at room temperature. Scale bar, $10\ \mu\text{m}$. **(D)** Time-lapse fluorescence images showing that GFP-SKAP ($10\ \mu\text{M}$) droplets rapidly fuse upon contact into one spherical droplet. The droplet formation buffer (BRB80) contains 3% PEG-8000. Scale bar, $2\ \mu\text{m}$. **(E)** Time-lapse images from the FRAP experiment. GFP-SKAP droplet in **C** was photobleached and fluorescence recovery was monitored; the white dotted box indicates the bleached area. Representative images at indicated time points are shown. Scale bar, $5\ \mu\text{m}$. **(F)** Normalized FRAP recovery curves for GFP-SKAP droplet in **E**. Data are mean \pm SEM at each time point; $n = 9$ coacervates, combined data from three independent repeats. **(G)** 1,6-hexanediol disrupts droplet formation by SKAP. Droplet formation was performed with GFP-SKAP ($10\ \mu\text{M}$ in BRB80 buffer with 3% PEG-8000) at room temperature in the presence or absence of 5% Hex. Scale bar, $10\ \mu\text{m}$. **(H)** Quantification of the size and number of droplets are shown. Each dot represents a droplet. Droplets in $n = 3$ fields ($130 \times 130\ \mu\text{m}^2$) in each group were quantified. Data represent mean \pm SEM and statistical significance was tested by two-sided *t*-test; $***P < 0.001$. **(I)** Phase diagram of GFP-SKAP in BRB80 buffer with indicated protein and salt concentrations. Analysis was performed after 5 min of incubation at room temperature. Green dots indicate condensates and 'x' indicates no condensates.

imaging of coacervate formation demonstrated the dynamics of SKAP droplets as they underwent fusion over time (Figure 2D).

To determine whether SKAP protein in the droplets exchanged with SKAP in the surrounding buffer, we performed fluorescence recovery after photobleaching (FRAP) of GFP-SKAP droplets *in vitro*. We observed a slow exchange of SKAP protein ($t_{1/2} = 48.3$ sec; Figure 2E and F). Interestingly, these exchange dynamics were similar to what had been measured for SKAP *in vivo* (Wang et al., 2012). To test whether hydrophobic interaction underlines SKAP phase separation, we added 1,6-hexanediol (5% Hex) into phase separation assay *in vitro*. As shown in Figure 2G and H, SKAP droplets were minimized by treatment of 5% Hex, suggesting that hydrophobic interaction is likely responsible for droplet formation.

To categorize the conditions dependent on the formation of SKAP droplets, we conducted experiments from two aspects: protein concentration and salt concentration. By varying protein concentrations, we found that a higher concentration of GFP-SKAP formed larger droplets with a higher efficiency evident by a larger number of droplets (Supplementary Figure S2A and B). Importantly, the property of SKAP phase behavior was attenuated by increased salt concentrations (Supplementary Figure S2C and D). Thus, we tested the effect of ion concentration on concentration-induced SKAP condensation (Figure 2I). Based on those analyses, we conclude that coacervate formation by SKAP may explain its dynamic interactions with Aurora B at kinetochores.

SKAP coacervates enrich Aurora B *in vitro*

The mechanisms underlying the localization of SKAP and Aurora B remained elusive despite intensive investigation (Shrestha et al., 2017). To test whether SKAP can recruit Aurora B into coacervates *in vitro*, we mixed mCherry-Aurora B with preformed GFP-SKAP coacervates and observed the partition of mCherry-Aurora B. Although mCherry-Aurora B does not form droplets, addition of mCherry-Aurora B resulted in recruitment of mCherry-Aurora B into preformed GFP-SKAP coacervates, suggesting that SKAP cooperates with Aurora B (Figure 3A). To determine whether SKAP protein in the droplets promote molecular dynamics of Aurora B in the droplets, we performed FRAP of GFP-SKAP and mCherry-Aurora B in the co-droplets *in vitro*. We observed a similar exchange of SKAP protein in the presence of Aurora B ($t_{1/2} = 57$ sec; Figure 3B and C). The exchange dynamics of SKAP were similar to what had been measured for SKAP alone *in vitro* (Figure 2F). However, the exchange dynamics of Aurora B in the same droplets were much slower ($t_{1/2} = 70$ sec; Figure 3C) to that of SKAP molecules. Interestingly, the coacervate property of Aurora B into SKAP droplets is sensitive to increased concentration of potassium, as 150 mM KCl attenuated the LLPS activity of SKAP (Figure 3D). As shown in Figure 3E, statistical analyses show that coacervate property of Aurora B into SKAP droplets was sensitive to salt. Thus, we conclude that Aurora B phase-separates into SKAP coacervates *in vitro*.

SKAP–Aurora B coacervates depend on C-terminal SKAP

To examine which region is necessary for SKAP phase separation, we constructed N-terminal SKAP (SKAP-NT) and C-terminal SKAP (SKAP-CT) as illustrated in Figure 4A. The bacterially recombinant proteins of SKAP were purified and analyzed by SDS–PAGE (Supplementary Figure S3A). We observed comparable droplet number and size of SKAP-CT phase separation with full-length SKAP (SKAP-FL) under conditions of the same protein concentration (10 μ M) in the presence of the molecular crowding agent (PEG) (Figure 4B). SKAP-NT failed to form droplets *in vitro* at the same condition (Figure 4B). Similar to what was observed in the full-length protein, SKAP-CT droplets exhibited sensitivity to higher concentration of salts (Supplementary Figure S3B and C). To determine the SKAP-CT protein exchange rate in the droplets, we performed FRAP analyses of GFP-SKAP-CT droplets *in vitro* (Figure 4C). Although the efficiency of FRAP was lower for SKAP-CT compared to SKAP-FL, we observed a faster exchange rate of SKAP-CT ($t_{1/2} = 34.8$ sec for SKAP-CT whereas $t_{1/2} = 48.3$ sec for SKAP-FL; Figure 4C and D). Consistent with what was seen in the SKAP-FL coacervates, SKAP-CT droplets also recruited Aurora B *in vitro* (Figure 4E). SKAP-NT failed to form coacervates alone or in the presence of Aurora B (Figure 4E). In this regard, SKAP-NT is a defective mutant in phase separation. Our FRAP analyses show that SKAP-CT and Aurora B molecules were dynamic, as they exhibited relatively fast turnover (Figure 4F), indicating that SKAP-CT specifies the recruitment of Aurora B into SKAP droplets (Figure 4G). As a control, increased salt concentration perturbed coacervates formed by SKAP-CT and Aurora B (Supplementary Figure S3D and E). Thus, we conclude that SKAP–Aurora B can undergo phase separation *in vitro* and the coacervates depend on SKAP-CT.

The phase-separation property of SKAP is important for its mitotic function

To study the phase-separation property of SKAP–Aurora B in mitosis, we used the Cry2 optoDroplet system to test whether SKAP can undergo phase separation *in vivo* (Shin et al., 2017). A phase-separating protein fused to the light-inducible dimerizing protein Cry2 will form droplets/punctae *in vivo* after exposure to blue light (Figure 5A). Majority of the COS-7 cells expressing SKAP-mCherry-Cry2 and SKAP-CT-mCherry-Cry2 formed distinct puncta in interphase nuclei after exposure to blue light (Figure 5B; Supplementary Figure S4A). By contrast, none of the cells expressing SKAP-NT-mCherry-Cry2 formed foci (Supplementary Figure S4A). Inhibition of weak hydrophobic interactions by the aliphatic alcohol 1,6-hexanediol disrupts many phase-separated compartments in cells (Trivedi et al., 2019). To test whether the SKAP phase-separated droplets possess characteristic protein of hydrophobic interactions, an aliquot of 1,6-hexanediol (5% Hex) was added into live cells, and addition of 5% Hex disrupted Opto-SKAP droplet in live cells (Figure 5C) as it did for GFP-SKAP droplets *in vivo* (Figure 5D).

We already identified LLPS-deficient SKAP (SKAP-NT). To study the effect of SKAP LLPS property in mitosis, we introduced wild-

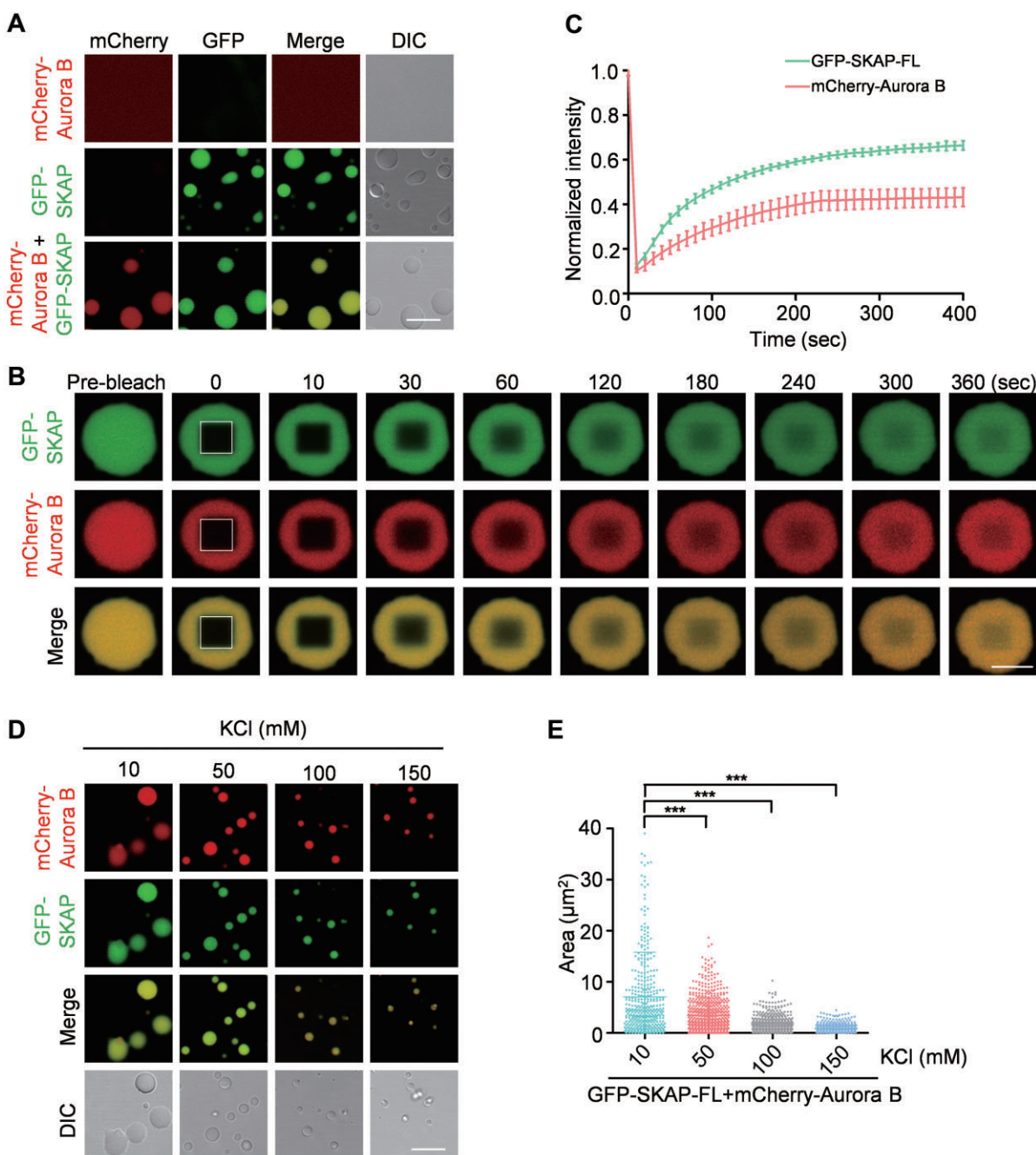


Figure 3 Characterization of SKAP and Aurora B co-condensation. **(A)** *In vitro* co-droplet formation assay. mCherry-Aurora B ($10 \mu\text{M}$) either alone or mixed together with $10 \mu\text{M}$ GFP-SKAP was analyzed using droplet formation assay under the same condition as described in Figure 2C. The droplet formation buffer (BRB80) contains 3% PEG-8000. Scale bar, $10 \mu\text{m}$. **(B)** Time-lapse images from the FRAP experiment. SKAP and Aurora B heterogeneous coacervates in **A** were photobleached and fluorescence recovery was monitored; the white dotted box indicates the bleached area. Representative images at indicated time points are shown. Scale bar, $5 \mu\text{m}$. **(C)** Graph of fluorescence recovery after photobleaching inside the droplet over time. Data are mean \pm SEM at each time point; $n = 9$ coacervates, combined data from three independent repeats. **(D)** Representative images of droplet formation of GFP-SKAP ($10 \mu\text{M}$) and mCherry-Aurora B ($10 \mu\text{M}$) in droplet formation buffer (BRB80) with varying concentrations of salt and 3% PEG. Scale bar, $10 \mu\text{m}$. **(E)** Quantification of the size and number of droplets are shown. Each dot represents a droplet. Droplets in $n = 3$ fields ($130 \times 130 \mu\text{m}^2$) in each group were quantified. Data represent mean \pm SEM and statistical significance was tested by two-sided *t*-test; *** $P < 0.001$.

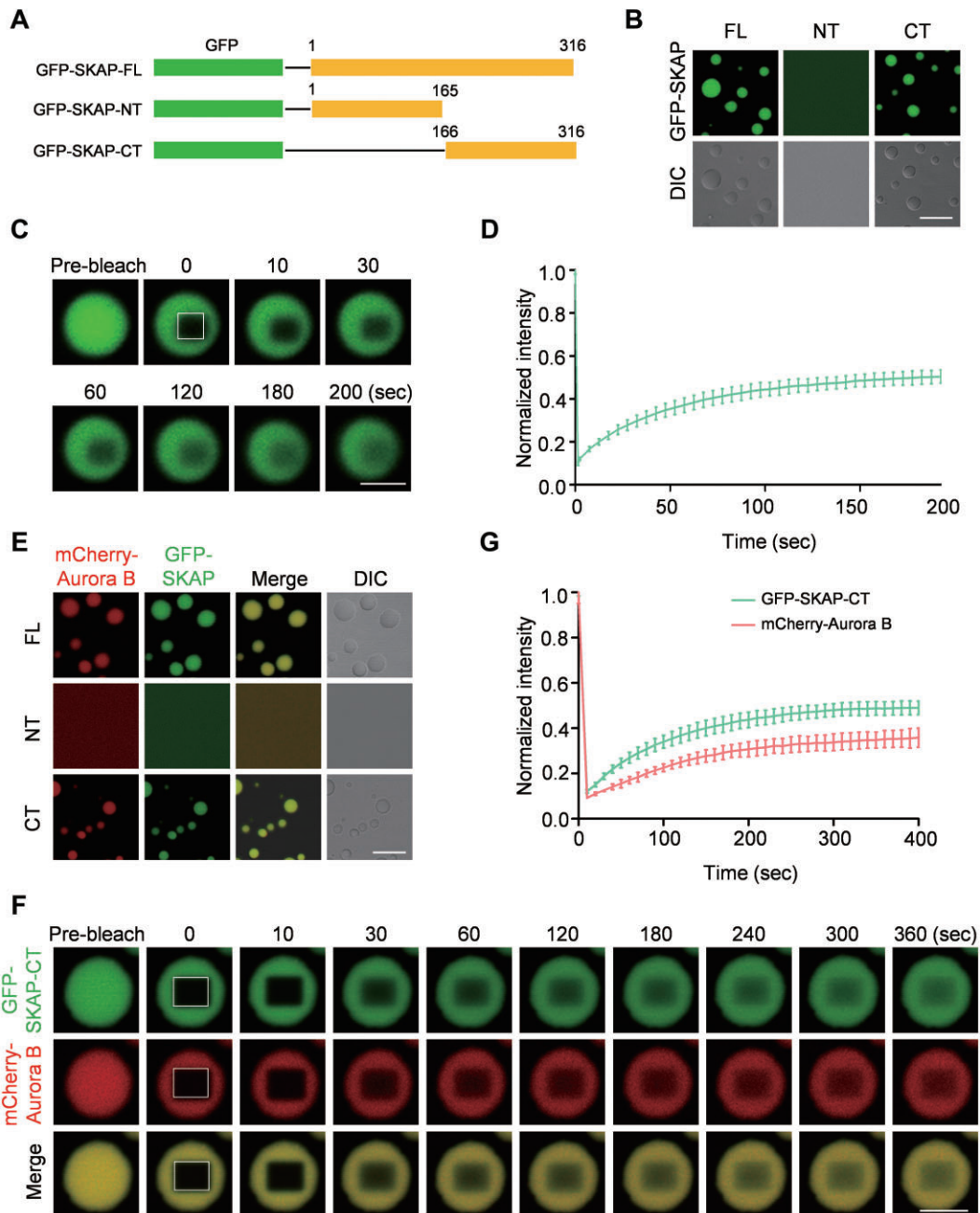


Figure 4 SKAP-CT is responsible for phase separation and Aurora B recruitment. **(A)** Schematic drawing of SKAP truncation mutants. Residue numbers at domain boundaries are indicated. **(B)** *In vitro* droplet formation assay. GFP-SKAP-FL (10 μ M), GFP-SKAP-NT (10 μ M), and GFP-SKAP-CT (10 μ M) were analyzed using a droplet formation assay under the same condition as described in Figure 2C. The droplet formation buffer (BRB80) contains 3% PEG-8000. Scale bar, 10 μ m. **(C)** Time-lapse images from the FRAP experiment. GFP-SKAP-CT coacervates in **B** were photobleached and fluorescence recovery was monitored; the white dotted box indicates the bleached area. Representative images at indicated time points are shown. Scale bar, 5 μ m. **(D)** Graph of fluorescence recovery after photobleaching inside the droplet over time. Data are mean \pm SEM at each time point; $n = 9$ coacervates, combined data from three independent repeats. **(E)** *In vitro* co-droplet formation assay. mCherry-Aurora B (10 μ M) mixed together with 10 μ M GFP-SKAP-FL, GFP-SKAP-NT, or GFP-SKAP-CT was analyzed using droplet formation assay under the same condition as described in Figure 2C. The droplet formation buffer (BRB80) contains 3% PEG-8000. Scale bar, 10 μ m. **(F)** Time-lapse images from the FRAP experiment. GFP-SKAP-CT and mCherry-Aurora B heterogeneous coacervates in **E** were photobleached together and fluorescence recovery was monitored; the white dotted box indicates the bleached area. Representative images at indicated time points are shown. Scale bar, 5 μ m. **(G)** Graph of fluorescence recovery after photobleaching inside the droplet over time. Data are mean \pm SEM at each time point; $n = 9$ coacervates, combined data from three independent repeats.

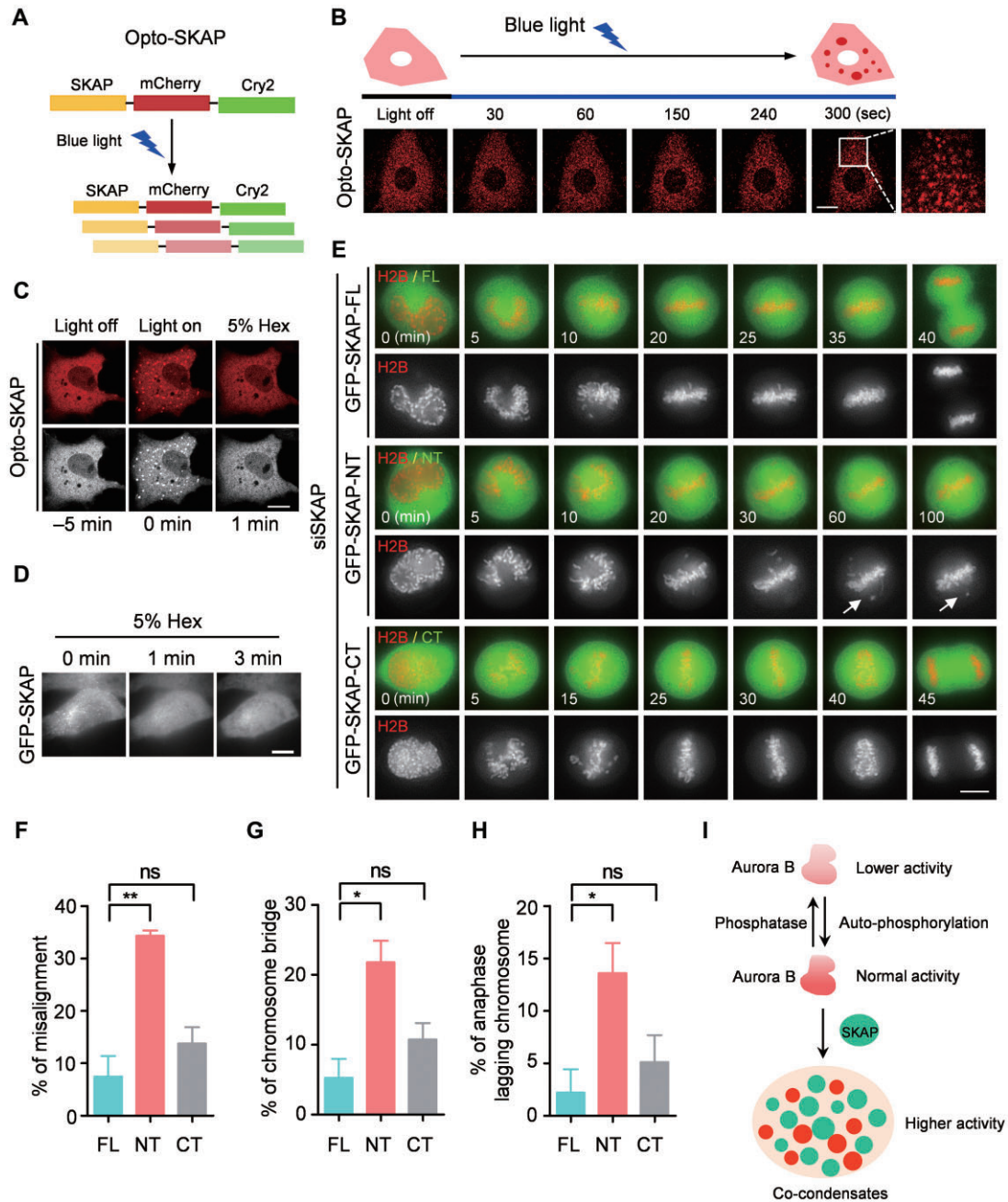


Figure 5 Phase separation-deficient truncation of SKAP leads to mitotic defects. **(A)** Schematic diagram of the optogenetic system. The ‘opto-SKAP’ construct consists of SKAP fused to mCherry fluorescent protein and the Cry2PHR domain. **(B)** Blue light activation of opto-SKAP-FL leads to rapid clustering in living COS-7 cells. Representative fluorescence images of light-activated assembly of opto-SKAP are shown. Images were taken every 10 sec. Scale bar, 20 μ m. **(C)** 1,6-hexanediol disrupts opto-SKAP clustering in cells. COS-7 cells were treated with 5% Hex after blue light activation of opto-SKAP. Images were taken every 10 sec. Scale bar, 20 μ m. **(D)** Overexpression of GFP-SKAP in HeLa cell forms droplet-like cluster, which is disrupted by 5% Hex treatment. HeLa cells transfected with GFP-SKAP were treated with 5% Hex. Images were taken at indicated time points. Scale bar, 10 μ m. **(E)** Representative mitotic phenotypes in HeLa cells expressing siSKAP along with GFP-SKAP-FL or truncations (FL/NT/CT in green color) resistant to siSKAP were shown by DeltaVision time-lapse microscopy, visualized with mCherry-H2B (H2B in red color) (arrows, misalignment; numbers at bottom left of images indicate elapsed time in minutes). Scale bar, 10 μ m. **(F–H)** Quantification of chromosome segregation defects of live HeLa cells in **E**. At least 30 cells were analyzed from three independent experiments for each construct ($n = 40$, GFP-SKAP-FL; $n = 37$, GFP-SKAP-NT; $n = 38$, GFP-SKAP-CT). Data represent mean \pm SEM and were examined with two-sided t -test; * $P < 0.05$, ** $P < 0.01$, n.s. (non-significant) indicates $P > 0.05$. **(I)** The model for Aurora B kinase activity regulated by SKAP phase separation.

type and LLPS-deficient SKAP into HeLa cells depleted of endogenous SKAP. Our real-time imaging analyses show that cells expressing full-length and LLPS-competent SKAP progressed into and through mitosis faithfully (Figure 5E, top and bottom panels). However, cells expressing LLPS-deficient SKAP exhibited characteristic phenotype of chromosome misalignment, lagging chromosomes, and chromatid bridges (Figure 5E, middle panels, arrows). Our statistical analyses of three independent preparations indicate that expression of SKAP deficient of LLPS resulted in significant increases in chromosome segregation errors such as chromosome misalignment, lagging chromosomes, and chromatid bridges (Figure 5F–H). Thus, we conclude that the phase-separation property of SKAP is important for correcting kinetochore–microtubule attachments and maintaining the end-on capture of kinetochore microtubules.

Discussion

The kinetochore is a complex molecular machinery to power chromosome movements by coupling kinetochore–microtubule dynamics. Proper alignment and segregation of sister chromatids during mitosis require accurate end-on capture. To build effective kinetochore–microtubule attachment, it must satisfy two criteria: one is to maintain the dynamic flux of kinetochore microtubules, and the other is to secure the dynamic link between the kinetochore and microtubules. Our early studies revealed that SKAP interacts directly with structural determinant of the kinetochore through its C-terminal contacts with MIS13 (Yang et al., 2008; Wang et al., 2012). Together with our early demonstration that N-terminal region of SKAP binds to microtubule plus-ends (Wang et al., 2012), our present discovery that SKAP-CT possesses LLPS property essential for Aurora B-elicited error correction establishes an exciting working model, in which compartmentalization of Aurora B in SKAP at the kinetochore serves as novel end-on capture machinery for dynamic kinetochore–microtubule orchestration in mitosis (Figure 5I).

It was recently reported that Aurora B kinase serves as a key regulator for end-on conversion by regulating Astrin–SKAP complex through a multi-step end-on conversion process (Shrestha et al., 2017). However, the currently available evidence provides little well-defined information regarding the molecular basis underlying SKAP-coupled interface of kinetochore–microtubule. Our study present here supports the notion of SKAP-elicited end-on capture model and establishes an interesting compartment constituted by SKAP phase separation at the outer kinetochore, which provides rapid pool of Aurora B kinase for accurate error correction. Since several lines of related works including our own have established the role of Aurora B–MIS13–SKAP signaling in the error correction (Yang et al., 2008; Petrovic et al., 2014, 2016; Volkov et al., 2018), it would be of great interest in the follow-up studies to illuminate how Aurora B kinase acts in the SKAP-constituted compartment for spindle microtubule attachment errors.

Recent studies unraveled the role of LLPS-driven compartments in inner centromere signaling and spindle matrix assembly (Jiang et al., 2015), implying the general involvements of LLPS-driven regulation in mitosis. In fact, recent studies suggest that BuGZ coacervation promotes Aurora A activation in mitosis (Huang et al., 2018; Woodruff, 2018), suggesting that compartmentalization of mitotic regulators are essential for accurate chromosome segregation. It is worth noting that SKAP LLPS appears negatively regulated by increased concentration of potassium chloride *in vitro*. In fact, the small size of SKAP droplets seen in *in vitro* reconstitution assay at physiological level of potassium is consistent with our proposed function for SKAP LLPS in mitosis, which provides a dynamic compartment for prompt catalysis of SKAP–Aurora B interaction and activity. Despite the fact that SKAP-NT exhibits LLPS-deficiency property *in vitro* and perturbation of mitosis *in vivo*, it would be of great interest down the road to distinguish the LLPS-driven function of SKAP from its classical properties.

In addition, it was also demonstrated that the dual-specificity kinase DYRK3 acts as a central dissolvase of several types of membraneless organelle during mitosis (Rai et al., 2018). Given the fact that the kinetochore plasticity and macromolecular assembly dynamics are guided by precise protein covalent modifications, such as phosphorylation, acetylation, and methylation, it will be exciting to visualize how mitosis-elicited post-translational modifications control the compartmentalization of dynamic kinetochore assembly during cell division using fluorescence resonance energy transfer-based optical reporter combined with spectral imaging (Thein et al., 2007; Valm et al., 2017; Liu et al., 2020). Along with this line, it would be of great interest to evaluate whether SKAP coacervates selectively recruit active Aurora B kinase into the droplets and how this type of compartmentalization provides spatiotemporal catalysis of Aurora B activity during mitosis.

In summary, we show that SKAP undergoes spontaneous phase separation via its C-terminal tail. SKAP and Aurora B form heterogenous coacervates *in vitro*, and LLPS-driven SKAP interaction with Aurora B is essential for accurate chromosome segregation and alignment. Our present study refines the current working model of core kinetochore–microtubule attachment and proposes LLPS-driven end-on capture model for accurate chromosome segregation in mitosis. Further molecular delineation of MIS13–SKAP–Aurora B function in the outer kinetochore will uncover the underlying regulatory basis for temporal control of centromere plasticity during mitosis and the defective processes underlying aneuploidy.

Materials and methods

Construction of plasmids

To generate His-GFP-SKAP full-length and truncation mutants, SKAP was amplified together with GFP from pEGFP-C1-SKAP

plasmid by polymerase chain reaction (PCR) and cloned into the pET-22b (+) vector (Novagen) by DNA homologous recombination method. To generate Aurora B-mCherry-His, Aurora B gene was cloned into pET-22b (+) vector by DNA homologous recombination method, followed by PCR-amplified mCherry gene insertion by *Bam*HI and *Xho*I digestion. OptoSKAP plasmid (SKAP-mCherry-Cry2) was constructed by replacing FUSN by SKAP in pHR-FUSN-mCh-Cry2WT plasmid (addgene 101223). The GFP-SKAP full-length and truncation mutants were generated by inserting PCR-amplified SKAP-FL/NT/CT into pEGFP-C1 (Clontech). All plasmids used were verified by sequencing.

Protein expression and purification

All recombinant proteins were expressed in *E. coli* BL21 (DE3). The bacteria were grown in LB medium at 37°C, and protein expression was induced at 16°C with 0.1 mM isopropyl β -D-1-thiogalactopyranoside for 16 h. For His-tagged recombinant proteins, the bacteria were suspended and lysed by sonication in Ni-NTA binding buffer (50 mM NaH₂PO₄, pH 8.0, 300 mM NaCl, and 10 mM imidazole) and incubated with Ni-NTA agarose (QIAGEN) for 1.5 h at 4°C. The agarose was washed three times in Ni-NTA binding buffer supplemented with 20 mM imidazole and eluted with Ni-NTA binding buffer supplemented with 250 mM imidazole. For GST-tagged recombinant proteins, the bacteria were suspended and lysed by sonication in phosphate-buffered saline (PBS) buffer supplemented with 0.5% Triton X-100. The preparation was incubated with glutathione-Sepharose 4B (GE Healthcare Life Science) for 1.5 h at 4°C. The resin was washed three times in PBS buffer supplemented with 0.5% Triton X-100. All purification procedures were carried out at 4°C, and a protease inhibitor mixture (Sigma) and phenylmethanesulfonyl fluoride were added to prevent protein degradation.

Cell culture and drug treatment

HeLa and COS-7 cells from the American Type Culture Collection were maintained in advanced Dulbecco's modified Eagle's medium (Gibco) with 10% fetal bovine serum (FBS; Hyclone) and penicillin–streptomycin (100 units/ml and 100 μ g/ml, respectively; Gibco) at 37°C with 8% CO₂.

For cell cycle synchronization, HeLa cells were first blocked in G1/S with 2.5 mM thymidine (Sigma) for 16 h and then released in fresh culture medium for 8 h to enrich mitotic cells. To inhibit Aurora B kinase activity, cells were treated with the Aurora B inhibitor ZM447439 (2458, TOCRIS) at 5 μ M for 45 min after thymidine release.

Transfection and siRNA

All plasmids and siRNAs were transfected into cells using Lipofectamine 2000 or Lipofectamine 3000 (Invitrogen) according to the manufacturer's instructions. SKAP siRNA target sequence was 5'-AGGCTACAAACCACTGAGTAA-3' (L-60262, GenePharma).

Antibody

According to standard protocols, rabbit antibodies against SKAP were prepared using full-length recombinant proteins from bacteria as described previously (Wang et al., 2004). The following antibodies were obtained from commercial sources: anti- α -tubulin (ab80779, 1:5000) was from Abcam; anti-pS10-H3 (3377, 1:1000 for western blotting, 1:100 for immunofluorescence), anti-His-tag (12698, 1:2000), and anti-EB1 (2164, 1:1000) antibodies were from Cell Signaling Technology; anti-pT232-Aurora B antibody (600-401-677, 1:2000 for western blotting, 1:200 for immunofluorescence) was from Rockland; anti-Aurora B (AIM-1, 1:2000) antibody was from BD Biosciences; secondary antibodies were from Jackson ImmunoResearch Laboratory.

IP and pull-down assays

For IP, HeLa cells were synchronized at mitosis before being trypsinized and lysed in IP buffer (50 mM Tris-HCl, pH 8.0, 150 mM NaCl, and 0.1% Triton X-100) supplemented with protease inhibitor cocktail (Sigma) and phosphatase inhibitor cocktail (Sigma). After pre-clearing with protein A/G resin, the lysate was incubated with SKAP antibody at 4°C for 24 h with gentle rotation. Protein A/G resin was then added to the lysate and incubated for another 6 h. The protein A/G resin was then spun down and washed three times with lysis buffer before being resolved by SDS–PAGE and immunoblotted with the indicated antibodies.

For pull-down assay, GST and GST fusion protein-bound sepharose beads were separately incubated for 2 h with purified His-tagged fusion proteins expressed in *E. coli* cells on ice in PBS containing protease inhibitor cocktail and 0.1% Triton X-100. After the incubation, the sepharose beads were washed for three times with PBS containing 0.1% Triton X-100 and once more with PBS. Then the beads were boiled in SDS–PAGE sample buffer. The bound proteins were separated on SDS–PAGE and detected by western blotting.

Immunofluorescence and live cell imaging

For immunofluorescence, HeLa cells were plated onto a sterile 24-well plate (Corning Glass Works) for transfection or drug treatment and fixed with 3.7% formaldehyde in PBS for 10 min at 37°C. In order to facilitate the staining of the antibody into the cells, the treated and fixed cells were permeated with PBS containing 0.1% Triton X-100 for 5 min. After blocking with PBS with 0.05% Tween-20 buffer containing 1% bovine serum albumin (Sigma) for 45 min at room temperature, the fixed cells were incubated with primary antibodies in a humidified chamber for 1 h at room temperature or overnight at 4°C, followed by secondary antibodies for 1 h at 37°C. The DNA was stained with 4',6-diamidino-2-phenylindole from Sigma. Images were captured by DeltaVision softWoRx software (Applied Precision) and processed by deconvolution and z-stack projection.

For time-lapse imaging, HeLa cells were cultured in glass-bottom culture dishes (MatTek) and maintained in CO₂-independent media (Gibco) supplemented with 10% FBS and 2 mM glutamine (Mo et al., 2016). During imaging, the dishes were placed in a sealed chamber at 37°C. Images of living cells were taken with a DeltaVision microscopy system.

Phase separation assay

Purified proteins were diluted to varying concentrations in BRB80 buffer (pH 6.8) containing 80 mM PIPES, 1 mM MgCl₂, and 1 mM EGTA with the indicated salt concentrations. Protein solution (10 μl) was loaded onto a glass slide and imaged using an LSM880 microscope (Zeiss). Then, 3% PEG-8000 (Sangon Biotech, A600433) was added in phase separation assays; 1,6-hexanediol (Sigma, 88571) was used at 5%.

Droplet area measurement

Image J (NIH) was used to identify droplets and characterize their number and size. Droplets were quantified in a 130 × 130 μm² field with equal threshold (>5-pixel minimum droplet size), and droplet area was identified using the Binary Watershed function and Analyze Particles function of Image J.

OptoDroplet assay

OptoSKAP assay was carried out as described previously (Shin et al., 2017). SKAP-mCherry-Cry2 was transfected into COS-7 cells 24 h after plating into glass-bottom culture dishes (MatTek). Twenty-four hours after transfection, the cells were imaged using a Zeiss 880 laser confocal scanning microscope with a 63× Plan-Apochromat 1.4 oil immersion lens in a humidified chamber maintained at 37°C in the presence of 5% CO₂. To induce phase separation, cells were exposed to 488-nm-wavelength light every 10 sec, and single z-plane images were taken in the 568 nm channel to observe droplet formation.

FRAP analysis

GFP-tagged SKAP proteins were used to label liquid droplets *in vitro*. FRAP experiments were performed on a confocal microscope (LSM 880, Zeiss) at room temperature. Defined regions were photobleached at 488 nm and the fluorescence intensities in these regions were collected every 1 sec and normalized to the initial intensity before bleaching. Image intensity was measured by mean region of interest and further analyzed by Prism (GraphPad).

Statistics

All statistics are described in the figure legends. Two-sided unpaired Student's *t*-test was applied for experimental comparisons, using GraphPad Prism. All western blotting analyses were

taken from three separated experiments. No statistical method was used to predetermine sample size. All data were expected to have normal distribution.

Supplementary material

Supplementary material is available at *Journal of Molecular Cell Biology* online.

Acknowledgements

The authors thank their laboratory members for inspiring discussion during the course of this study and Mingrui Ding for input in the early stage of this project.

Funding

This work was supported in part by grants from the National Natural Science Foundation of China (32090040, 31621002, 21922706, 91854203, 91853115, 81630080, 31430054, 31471275, 31871359, 31970655, and 31671405), the National Key Research and Development Program of China (2017YFA0503600, 2016YFA0100500, and 2017YFA0102900), the Ministry of Education (IRT_17R102), The Strategic Priority Research Program of Chinese Academy of Sciences (XDB19000000), the Fundamental Research Funds for the Central Universities (WK2070000066 and WK2070000194), and National Institutes of Health Grants (CA164133, DK115812, and DK56292).

Conflict of interest: none declared.

References

- Bakhroum, S.F., Genovese, G., and Compton, D.A. (2009a). Deviant kinetochore microtubule dynamics underlie chromosomal instability. *Curr. Biol.* *19*, 1937–1942.
- Bakhroum, S.F., Thompson, S.L., Manning, A.L., et al. (2009b). Genome stability is ensured by temporal control of kinetochore–microtubule dynamics. *Nat. Cell Biol.* *11*, 27–35.
- Banani, S.F., Lee, H.O., Hyman, A.A., et al. (2017). Biomolecular condensates: organizers of cellular biochemistry. *Nat. Rev. Mol. Cell Biol.* *18*, 285–298.
- Bao, X., Liu, H., Liu, X., et al. (2018). Mitosis-specific acetylation tunes Ran effector binding for chromosome segregation. *J. Mol. Cell Biol.* *10*, 18–32.
- Cheeseman, I.M. (2014). The kinetochore. *Cold Spring Harb. Perspect. Biol.* *6*, a015826.
- Cheeseman, I.M., and Desai, A. (2008). Molecular architecture of the kinetochore–microtubule interface. *Nat. Rev. Mol. Cell Biol.* *9*, 33–46.
- Cleveland, D.W., Mao, Y., and Sullivan, K.F. (2003). Centromeres and kinetochores: from epigenetics to mitotic checkpoint signaling. *Cell* *112*, 407–421.
- DeLuca, J.G. (2010). Kinetochore–microtubule dynamics and attachment stability. *Methods Cell Biol.* *97*, 53–79.
- Fang, L., Seki, A., and Fang, G. (2009). SKAP associates with kinetochores and promotes the metaphase-to-anaphase transition. *Cell Cycle* *8*, 2819–2827.
- Foley, E.A., and Kapoor, T.M. (2013). Microtubule attachment and spindle assembly checkpoint signalling at the kinetochore. *Nat. Rev. Mol. Cell Biol.* *14*, 25–37.

- Hara, M., and Fukagawa, T. (2017). Critical foundation of the kinetochore: the constitutive centromere-associated network (CCAN). *Prog. Mol. Subcell. Biol.* *56*, 29–57.
- Huang, Y., Li, T., Ems-McClung, S.C., et al. (2018). Aurora A activation in mitosis promoted by BuGZ. *J. Cell Biol.* *217*, 107–116.
- Huang, Y., Lin, L., Liu, X., et al. (2019). BubR1 phosphorylates CENP-E as a switch enabling the transition from lateral association to end-on capture of spindle microtubules. *Cell Res.* *29*, 562–578.
- Huang, Y., Wang, W., Yao, P., et al. (2012). CENP-E kinesin interacts with SKAP protein to orchestrate accurate chromosome segregation in mitosis. *J. Biol. Chem.* *287*, 1500–1509.
- Hyman, A.A., Weber, C.A., and Julicher, F. (2014). Liquid–liquid phase separation in biology. *Annu. Rev. Cell Dev. Biol.* *30*, 39–58.
- Jiang, H., Wang, S., Huang, Y., et al. (2015). Phase transition of spindle-associated protein regulate spindle apparatus assembly. *Cell* *163*, 108–122.
- Li, P., Banjade, S., Cheng, H.C., et al. (2012). Phase transitions in the assembly of multivalent signalling proteins. *Nature* *483*, 336–340.
- Liu, X., Liu, X., Wang, H., et al. (2020). Phase separation drives decision making in cell division. *J. Biol. Chem.* *295*, 13419–13431.
- McKinley, K.L., and Cheeseman, I.M. (2016). The molecular basis for centromere identity and function. *Nat. Rev. Mol. Cell Biol.* *17*, 16–29.
- Mo, F., Zhuang, X., Liu, X., et al. (2016). Acetylation of Aurora B by TIP60 ensures accurate chromosomal segregation. *Nat. Chem. Biol.* *12*, 226–232.
- Petrovic, A., Keller, J., Liu, Y., et al. (2016). Structure of the MIS12 complex and molecular basis of its interaction with CENP-C at human kinetochores. *Cell* *167*, 1028–1040.e15.
- Petrovic, A., Mosalaganti, S., Keller, J., et al. (2014). Modular assembly of RWD domains on the Mis12 complex underlies outer kinetochore organization. *Mol. Cell* *53*, 591–605.
- Rai, A.K., Chen, J.X., Selbach, M., et al. (2018). Kinase-controlled phase transition of membraneless organelles in mitosis. *Nature* *559*, 211–216.
- Shin, Y., Berry, J., Pannucci, N., et al. (2017). Spatiotemporal control of intracellular phase transitions using light-activated optoDroplets. *Cell* *168*, 159–171.e14.
- Shrestha, R.L., Conti, D., Tamura, N., et al. (2017). Aurora-B kinase pathway controls the lateral to end-on conversion of kinetochore–microtubule attachments in human cells. *Nat. Commun.* *8*, 150.
- So, C., Seres, K.B., Steyer, A.M., et al. (2019). A liquid-like spindle domain promotes acentrosomal spindle assembly in mammalian oocytes. *Science* *364*, eaat9557.
- Thein, K.H., Kleylein-Sohn, J., Nigg, E.A., et al. (2007). Astrin is required for the maintenance of sister chromatid cohesion and centrosome integrity. *J. Cell Biol.* *178*, 345–354.
- Trivedi, P., Palomba, F., Niedzialkowska, E., et al. (2019). The inner centromere is a biomolecular condensate scaffolded by the chromosomal passenger complex. *Nat. Cell Biol.* *21*, 1127–1137.
- Valm, A.M., Cohen, S., Legant, W.R., et al. (2017). Applying systems-level spectral imaging and analysis to reveal the organelle interactome. *Nature* *546*, 162–167.
- Volkov, V.A., Huis In 't Veld, P.J., Dogterom, M., et al. (2018). Multivalency of NDC80 in the outer kinetochore is essential to track shortening microtubules and generate forces. *eLife* *7*, e36764.
- Wang, H., Hu, X., Ding, X., et al. (2004). Human Zwint-1 specifies localization of Zeste White 10 to kinetochores and is essential for mitotic checkpoint signaling. *J. Biol. Chem.* *279*, 54590–54598.
- Wang, X., Zhuang, X., Cao, D., et al. (2012). Mitotic regulator SKAP forms a link between kinetochore core complex KMN and dynamic spindle microtubules. *J. Biol. Chem.* *287*, 39380–39390.
- Woodruff, J.B. (2018). Phase separation of BuGZ promotes Aurora A activation and spindle assembly. *J. Cell Biol.* *217*, 9–10.
- Woodruff, J.B., Ferreira Gomes, B., Widlund, P.O., et al. (2017). The centrosome is a selective condensate that nucleates microtubules by concentrating tubulin. *Cell* *169*, 1066–1077.e10.
- Yang, Y., Wu, F., Ward, T., et al. (2008). Phosphorylation of HsMis13 by Aurora B kinase is essential for assembly of functional kinetochore. *J. Biol. Chem.* *283*, 26726–26736.
- Yang, Y., and Yu, H. (2018). Partner switching for Ran during the mitosis dance. *J. Mol. Cell Biol.* *10*, 89–90.
- Zachos, G. (2016). Cell division: TIPs for shaping Aurora B activity. *Nat. Chem. Biol.* *12*, 204–205.
- Zhao, G., Cheng, Y., Gui, P., et al. (2019). Dynamic acetylation of the kinetochore-associated protein HEC1 ensures accurate microtubule–kinetochore attachment. *J. Biol. Chem.* *294*, 576–592.